Transport of Multispecies Ion Crystals through a Junction in a Radio-Frequency Paul Trap

William Cody Burton[ORCID],[*] Brian Estey, Ian M. Hoffman[ORCID], Abigail R. Perry, Curtis Volin, and Gabriel Price[†]

Quantinuum, 303 South Technology Court, Broomfield, Colorado 80021, USA

We report on the first demonstration of transport of a multispecies ion crystal through a junction in a rf Paul trap. The trap is a two-dimensional surface-electrode trap with an X junction and segmented control electrodes to which time-varying voltages are applied to control the shape and position of potential wells above the trap surface. We transport either a single ^{171}Yb$^+$ ion or a crystal composed of a ^{138}Ba$^+$ ion cotrapped with the ^{171}Yb$^+$ ion to any port of the junction. We characterize the motional excitation by performing multiple round-trips through the junction and back to the initial well position without cooling. The final excitation is then measured using sideband asymmetry. For a single ^{171}Yb$^+$ ion, transport with a 4 m/s average speed induces between 0.013 ± 0.001 and 0.014 ± 0.001 quanta of excitation per round-trip, depending on the exit port. For a Ba-Yb crystal, transport at the same speed induces between 0.013 ± 0.001 and 0.030 ± 0.002 quanta per round-trip of excitation to the in-phase axial mode. Excitation in the out-of-phase axial mode ranges from 0.005 ± 0.001 to 0.021 ± 0.001 quanta per round-trip.

Trapped ions are one of the leading candidate systems for scalable quantum computers [1,2]. In a trapped-ion quantum computer, quantum information is stored in the internal atomic states of the qubit ions, and multiqubit gates are usually performed by coupling the internal states of two qubits with a common motional mode [3]. Qubit connectivity can be achieved through control of trapping potentials created by surface-electrode ion traps [4–6].

All-to-all connectivity can be achieved either by including all qubits in a single crystal [7] or by use of a quantum charge coupled device (QCCD) architecture [8,9], where gates are performed on small chains of ions, which can be reordered and reconfigured. Current trapped-ion quantum computers [7,9,10] use effectively one-dimensional (linear trap) geometries. In such linear traps, sorting ions between gates is done through a combination of potential well splits [11], rotations [12], and linear transports [11,13]. Sorting on two-dimensional grids additionally requires transport through junctions to connect linear sections. There have been demonstrations of ion transport through several junction geometries, including T junctions [14], wafer-trap [15,16] and surface [17] X junctions, and Y junctions [18–20]. In addition, optimizing the design of junction traps remains an active area of research [21,22]. However, there has been no reported effort to transport a multispecies ion crystal through the junction. Doing so allows for simultaneous transport of a sympathetic coolant ion with each qubit, simplifying the sorting algorithm in a large-scale quantum computer.

In this Letter, we present fast, low-excitation junction transport of both single ions and multispecies ion crystals through a microfabricated surface trap X junction fabricated

at Honeywell with a measurement zone on each leg of the junction (see Supplemental Material [23]). The coordinate system and zone names are shown in Fig. 1(a). For single species transport, we used a single ^{171}Yb$^+$ ion, and for multispecies transport, we used a crystal composed of one ^{138}Ba$^+$ ion cotrapped with one ^{171}Yb$^+$ ion (referred to as a Ba-Yb crystal in the remainder of this Letter). For both single species and multispecies transport, we were able to transport through the X junction to each of the legs and back to the starting position with low excitation, while preserving a deterministic crystal orientation. To our knowledge, this Letter presents the first transport with subquanta excitation through a junction in a surface trap of any crystal, as well as
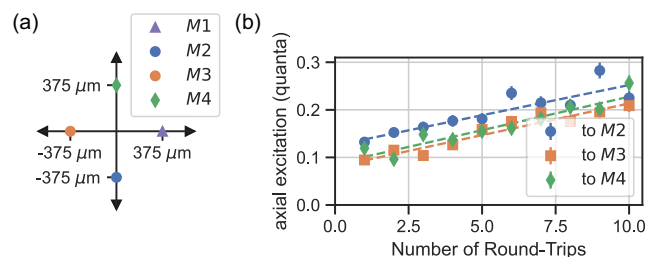

FIG. 1. (a) Zone names and coordinate system used in this Letter, with the junction at the origin and the four measurement zones: $M1$ at $(375, 0)$, $M2$ at $(0, -375)$, $M3$ at $(-375, 0)$, and $M4$ at $(0, 375)$ µm. (b) Measured axial excitation of a ^{171}Yb$^+$ ion after a variable number of round-trip transports from $M1$ through the junction to $M2$ (blue circles), $M3$ (orange squares), $M4$ (green diamonds), and back at an average speed of 4 m/s. Error bars are 1σ statistical uncertainty. The excitation is measured by sideband asymmetry on the axial mode.

the first transport of a multispecies crystal through a junction in any trap. Additionally, we studied the impacts of transport speed, amplitude drift of the rf drive, and external stray electric fields to ion excitation and ion loss.

Ion surface traps consist of two classes of electrodes: rf rails and segmented control electrodes. When a radio-frequency oscillating voltage is applied to the rf rails, charged particles in the vicinity undergo micromotion at the rf frequency. This interaction leads to an effective potential $\Phi_{pp}(\vec{x})$, known as the pseudopotential [1,27]. For each control electrode, we calculate a basis function $\Phi_i(\vec{x})$ that describes its contribution to the electrical potential at $\vec{x}$ when 1 V is applied to the electrode. The total potential is given by $\Phi(\vec{x}) = \Phi_{pp}(\vec{x}) + \sum_i V_i \Phi_i(\vec{x})$, where the V_i are the voltages applied to each control electrode. For a given target trapping well (e.g., a potential with a minimum at a defined location and a set of trap frequencies), we can solve for the V_i using a constrained optimization method [16,28]. To create a waveform of voltages that transports an ion between two locations, we solve for a series of potential wells along the transport path. We then interpolate between these solutions to generate the time-dependent waveform (see Supplemental Material [23]).

The laws of electrostatics place constraints on the sorts of potentials that can be generated. We define the total confinement $C = \nabla^2 \Phi \propto \sum_i \omega_i^2$, where ω_i is the frequency of the ith normal motional mode of harmonic oscillation of a single ion. Because the control electrodes necessarily produce fields with zero divergence, $C \equiv \nabla^2 \Phi_{pp}$ and depends only on the pseudopotential. In other words, no set of control voltages can change the total confinement at a given point—they can only redistribute frequency among modes. In an X junction, the total confinement along the pseudopotential minimum near the center of the junction is significantly lower than elsewhere in the trap [29]. Figure 2 shows the properties of the pseudopotential along several possible transport paths in our trap. The path of minimum pseudopotential is defined by minimizing $\Phi_{pp}(\vec{x})$ over y and z for each x along the $M1$–$M3$ legs and minimizing over x and z along the $M2$–$M4$ legs. We see in Fig. 2(b) that the total confinement along the path of minimum pseudopotential is about $1/8$ of its maximum value along the path. Transporting along this path would lead to low trapping frequencies and correspondingly greater heating and ion loss.

A successful strategy in surface trap junction transport involves moving the ion off of the path of minimum pseudopotential [17,20]. In contrast to [17], we define the path of constant total confinement (CTC) as a path directly below (in $\hat{z}$) the path of minimum pseudopotential, with a height that varies to keep C constant along the path. Therefore, the path of CTC traverses the junction through its center. We choose the value of C so that the path of CTC and the path of minimum pseudopotential intersect above the trap at $M1$. As seen in Fig. 2(a), the path of CTC near the junction center is significantly closer to the trap surface than the path of minimum pseudopotential.
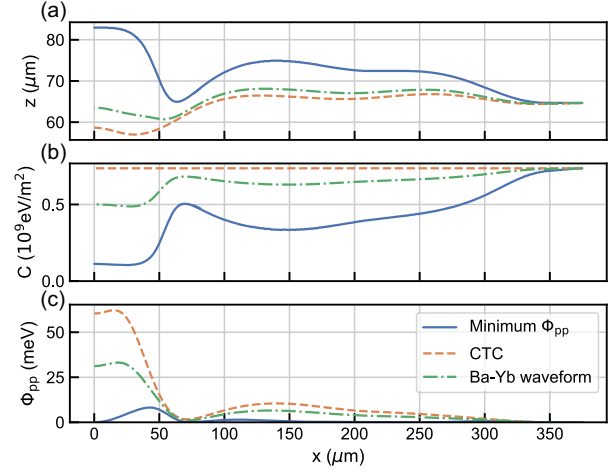

FIG. 2. Properties of the pseudopotential near the junction center along the path of minimum pseudopotential (solid blue line), the path of CTC (dashed orange line), and an intermediate path 80% of the way between the two (dot-dashed green line). For a single ^{171}Yb$^+$ ion, we constrain the total potential along the path of CTC, while for a Ba-Yb crystal, we use the intermediate path. The junction center is at $x = 0$ and the center of zone $M1$ is at $x = 375$ μm. (a) The height of each path above the surface of the trap. Note that the path of minimum pseudopotential and the path of CTC differ by ~ 20 μm at the junction center. (b) The total confinement (C) along each path. Along the path of minimum pseudopotential, C drops significantly, while by construction, it does not vary along the path of CTC. (c) Magnitude of the pseudopotential (Φ_{pp}) for a single ^{171}Yb$^+$ ion along each path. The local maximum around $x = 25$ μm is associated with anticonfinement in the axial direction.

For single species junction transport, we generated four waveforms that follow the path of CTC from the junction center to each of the measurement zones. We define the axial direction to be $\hat{x}$ for $M1$ and $M3$, and $\hat{y}$ for $M2$ and $M4$, and define the two perpendicular axes to be the radial directions. The total confinement along the path permits waveform solutions that maintain a constant axial trap frequency of 1.13 MHz and a large frequency separation of all motional modes over the entire trajectory, preventing transfer of excitation between the different motional modes [16]. In addition, we created two waveforms that rotate the principal axes of a single well at the center of the junction by 90°, which adiabatically convert the axial direction from $\hat{x}$ to $\hat{y}$ and back. The average speed of the transport can be set by linearly scaling the waveform playout in time.

Each single ion transport experiment begins with a ^{171}Yb$^+$ ion trapped in zone $M1$. We initialize the system by performing Doppler and sideband cooling [30] to cool all three motional modes to less than 0.1 quanta of excitation each. We then transport the ion to the center of the junction with the time-reversed junction-$M1$ waveform. To transport to $M3$, we apply the junction-$M3$ waveform. To transport to $M2$ or $M4$, we rotate the principal axes while the well center is stationary at the

center of the junction before applying the junction-$M2$ or junction-$M4$ waveform. We hold the well center position constant for 1 μs and then reverse the transport sequence back to $M1$. The final excitation is measured with Raman sideband asymmetry on the motional mode in the axial direction [30]. Measurements of transport with an average speed of 4 m/s are shown in Fig. 1(b). To separate nonzero initial temperature from excitation due to transport, we measure the excitation as a function of the number of round-trips and extract the slope, finding 0.013 ± 0.001, 0.013 ± 0.001, and 0.014 ± 0.001 quanta per round-trip to $M2$, $M3$, and $M4$, respectively. Because the transport path goes through regions of nonzero pseudopotential, amplitude noise on the rf drive can cause motional heating [15,16]. Our measured excitation values would be fully explained by a noise amplitude of −178 dBc at the axial trap frequency. This is consistent with measurements of the system electronics noise of −176 dBc at 1.13 MHz.

Multispecies crystals present a particular challenge for junction transport because the pseudopotential is proportional to the inverse of the ion mass [27], while the potential due to control electrodes only depends on the ion charge and is thus common to both species. This affects junction transport in two significant ways: (1) At approximately 25 μm from the center of the junction along the path of CTC, there is a local maximum of the pseudopotential [see Fig. 2(c)], which corresponds to an axial antitrapping potential. When making a transport waveform for a single ion species, our solution method takes this into account and holds the total axial curvature constant. However for the same waveform, an ion with a different mass will necessarily experience a changing axial curvature, which could lead to excess motional excitation or ion loss. (2) The minimum of the total potential for an ion of one mass occurs at the location where the gradient of the potential from the control electrodes is equal and opposite to the gradient of the pseudopotential. However, the potential minimum for a second ion with a different mass will be at a different position.

Given sufficient degrees of freedom by the control voltages, the total potential for both ion species could be independently controlled. However, this is experimentally impractical since the spacing of an ion crystal is generally on the order of a few micrometers, while the distance from the trap and the size of the control electrodes are both about 70 μm. Instead, we create multispecies junction transport waveforms through a numerical optimization process. We parametrize possible transport waveforms using 2 degrees of freedom: the path height parametrized by the fraction of the distance between the CTC and the pseudopotential minimum, and the potential curvature in the axial direction. These degrees of freedom have several coupled effects: (1) A larger axial curvature ensures that the total potential for both species remains trapping even at the peak of the anticurvature of the pseudopotential, but for a given total

confinement it reduces the potential curvature in the radial directions. (2) The path height affects both the total confinement and the gradient of the pseudopotential at the ion crystal. (3) The separation of the minima of the total potential for the different ion species is given by a combination of the gradient of the pseudopotential and the curvature in the vertical direction. Because of the nontrivial coupling, an exhaustive exploration of the parameter space was employed to find successful transport waveforms. At each search point in parameter space, the Ba-Yb waveforms are generated assuming a single synthetic ion with a mass equal to the average ion mass in the Ba-Yb crystal, following the defined transport path, and with a constant total potential curvature in the axial direction. We use a numerical equations-of-motion solver to simulate the behavior of a Ba-Yb crystal during transport in the test waveform, noting ion survival and nonadiabatic excitation. We found a broad region of low-excitation waveforms (see Supplemental Material [23]) in parameter space centered around an axial curvature of 9.1×10^7 eV/m^2 (equivalent to a 1.2 MHz axial frequency for the synthetic ion) and a path height 80% of the way between the path of minimum pseudopotential and the path of CTC (dot-dashed green line in Fig. 2). We use these parameters for multispecies junction transport for the data collected in the remainder of this Letter.

Figure 3 shows the experimental results for multispecies junction transport. We begin each experiment with a Ba-Yb crystal trapped in $M1$, with the ^{171}Yb$^+$ ion closer to the junction. A combination of electromagnetically induced transparency cooling on the ^{138}Ba$^+$ and sideband cooling on the ^{171}Yb$^+$ initializes the axial modes with less than 0.05 quanta of excitation and the radial modes with less than 0.3 quanta of excitation. As in the single species transport experiments, we perform a variable number of round-trips between $M1$ and the other three zones with an average speed of 4 m/s, for a round-trip time of 376 μs, before measuring the excitation in both axial motional modes (in phase and out of phase). The extracted slopes, reported in Table I, indicate that less than or equal to 0.03 quanta of excitation are added per round-trip. We should note that there is an oscillating residual with an amplitude of about 0.05 quanta on the out-of-phase mode excitation during transport to $M2$. As we discuss later, this could be caused by coupling from imperfectly cooled radial modes.

In addition, we examined the impact of transport speed on induced excitation, with results shown in Figs. 3(c) and 3(d). We find negligible excitation up to 6 m/s. Above this speed, we see evidence of coherent motional excitation in the in-phase mode, which is difficult to quantify with sideband asymmetry measurements. Finally, in the Supplemental Material [23], we report on the sensitivity of junction transport to drifts in the amplitude of the rf drive and to stray electric fields.
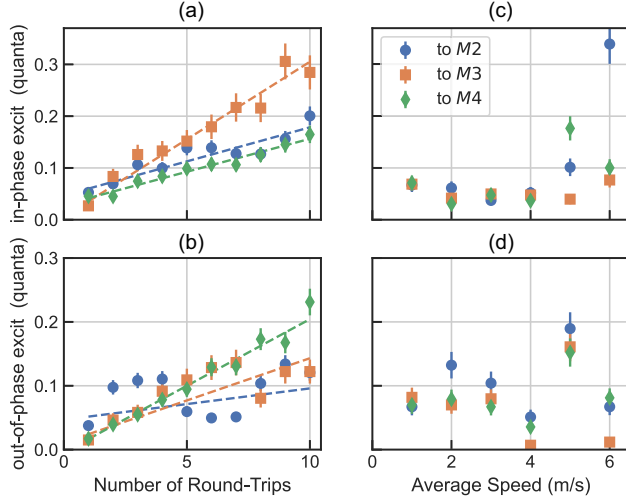
FIG. 3. Measured axial excitation of a Ba-Yb crystal after round-trip transports from $M1$ through the junction to $M2$ (blue circles), $M3$ (orange squares), $M4$ (green diamonds), and back. Error bars are 1σ statistical uncertainty. (a),(b) Excitation of the in-phase and out-of-phase motional modes after a variable number of round-trips without cooling. The extracted slopes are reported in Table I. (c),(d) Excitation of the in-phase and out-of-phase modes after one round-trip at a variable speed. The background heating rates of 29 ± 4 quanta/s for the in-phase mode and 3.0 ± 0.5 quanta/s for the out-of-phase mode are not subtracted from the data.
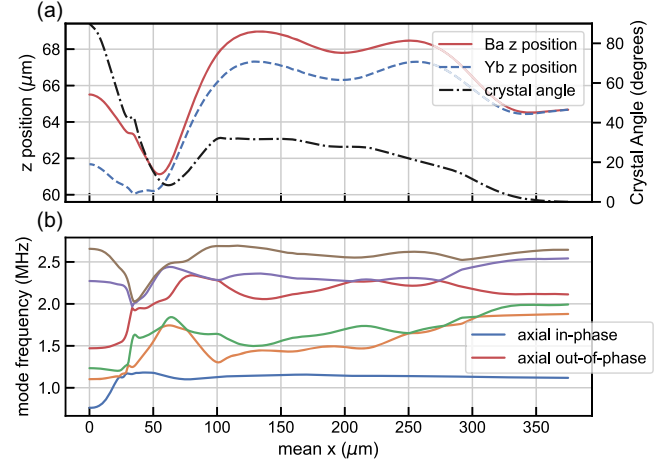

FIG. 4. Predicted properties of the Ba-Yb crystal during junction transport from $M1$ ($x = 375$ μm) to the junction center ($x = 0$) determined by numerical modeling of the equations of motion. (a) The left axis is the equilibrium height of the $^{138}\mathrm{Ba}^+$ (solid red line) and $^{171}\mathrm{Yb}^+$ ion (dashed blue line) above the trap surface, plotted versus the average x position of the two ions. The right axis is the angle of the crystal rotation relative to the xy plane (black dot-dashed line). The crystal starts in $M1$ with the $^{171}\mathrm{Yb}^+$ facing the junction and the $^{138}\mathrm{Ba}^+$ facing away (0°). At the junction center, the crystal is oriented perpendicular to the trap surface (90°). (b) Frequencies of the six normal motional modes of the crystal along the transport path. The axial modes in $M1$ are labeled. Several mode crossings during transport are predicted.

We numerically simulate the properties of a Ba-Yb crystal using the pseudopotential separately scaled by mass for each ion species. In Fig. 4(a), we plot the simulated equilibrium positions of a Ba-Yb crystal during transport from $M1$ to the junction center. (The qualitative features of this waveform are shared by all successful Ba-Yb wave-forms found in the numerical optimization.) When the crystal is near $M1$, where the trapping potential is similar to that generated in a linear surface trap, the crystal is oriented in the axial direction with the $^{171}\mathrm{Yb}^+$ ion closer to the junction. As the crystal approaches the center of the junction, due to different contributions to the total potential

TABLE I. Measured axial excitation per round-trip of a Ba-Yb crystal to the specified end zone and back to $M1$ at an average speed of 4 m/s. The excitation is measured by sideband asymmetry on the specified axial mode after a variable number of round-trips without cooling, and the slope and statistical uncertainty are reported below.

Crystal	Mode	Zone	Round-trip excitation (quanta)
Ba-Yb	In phase	$M2$	0.013 ± 0.001
Ba-Yb	In phase	$M3$	0.030 ± 0.002
Ba-Yb	In phase	$M4$	0.013 ± 0.001
Ba-Yb	Out of phase	$M2$	0.005 ± 0.001
Ba-Yb	Out of phase	$M3$	0.013 ± 0.001
Ba-Yb	Out of phase	$M4$	0.021 ± 0.001

from the pseudopotential, it rotates to be perpendicular to the trap (the $\hat{z}$ direction), regardless of the starting leg. When the crystal moves away from the junction center, either reversing its motion or moving into one of the other three legs, the crystal rotates back to a horizontal orientation, but always with the $^{171}\mathrm{Yb}^+$ closer to the junction, without an explicit rotation waveform. In Fig. 4(b), we plot the normal mode frequencies versus ion crystal location. Near $x = 25$ μm, there are several normal mode crossings that couple some of the radial modes to the axial modes during the transport. We have found that if we ground-state cool only the axial modes before transport (leaving the radial modes at the Doppler temperature), excitation is noticeably transferred into the axial modes, giving final axial excitations that are more complex to analyze. Therefore, in this Letter, we present only data that were taken with ground-state cooling of all modes before transport. Because of the mode coupling, the low final axial excitation is additionally a proxy measurement, suggesting low-excitation values in the radial modes as well.

In this Letter, we have presented the first low-excitation ion transport through a junction in a surface trap, completing the set of transport operations required in the QCCD architecture [9], as well as the first implementation of junction transport of a multispecies ion crystal, which provides an important tool for minimizing circuit times in a

two-dimensional ion trap quantum computer. We find that the transport adds very little excitation to all axial motional degrees of freedom at average speeds up to 6 m/s. In future work, further analysis of the waveform generation method and numerical optimization of the waveform may allow us to control or eliminate the crossing of motional modes during transport or to increase the speed of transport without additional coherent motional excitation [31]. In addition, to demonstrate scalability, we plan to develop the parallel transport of multiple ion crystals through neighboring junctions.

---

[*]william.burton@quantinuum.com

[†]gabriel.price@quantinuum.com

[1] D. J. Wineland, C. Monroe, W. M. Itano, D. Leibfried, B. E. King, and D. M. Meekhof, Experimental issues in coherent quantum-state manipulation of trapped atomic ions, J. Res. Natl. Inst. Stand. Technol. 103, 259 (1998).

[2] V. Kaushal, B. Lekitsch, A. Stahl, J. Hilder, D. Pijn, C. Schmiegelow, A. Bermudez, M. Müller, F. Schmidt-Kaler, and U. Poschinger, Shuttling-based trapped-ion quantum information processing, AVS Quantum Sci. 2, 014101 (2020).

[3] J. I. Cirac and P. Zoller, Quantum Computations with Cold Trapped Ions, Phys. Rev. Lett. 74, 4091 (1995).

[4] S. Seidelin, J. Chiaverini, R. Reichle, J. J. Bollinger, D. Leibfried, J. Britton, J. H. Wesenberg, R. B. Blakestad, R. J. Epstein, D. B. Hume, W. M. Itano, J. D. Jost, C. Langer, R. Ozeri, N. Shiga, and D. J. Wineland, Microfabricated Surface-Electrode Ion Trap for Scalable Quantum Information Processing, Phys. Rev. Lett. 96, 253003 (2006).

[5] D. Leibrandt, J. Labaziewicz, R. Clark, I. Chuang, R. Epstein, C. Ospelkaus, J. Wesenberg, J. Bollinger, D. Leibfried, D. Wineland et al., Demonstration of a scalable, multiplexed ion trap for quantum information processing, Quantum Inf. Comput. 9, 901 (2009).

[6] S. A. Schulz, U. Poschinger, F. Ziesel, and F. Schmidt-Kaler, Sideband cooling and coherent dynamics in a micro-chip multi-segmented ion trap, New J. Phys. 10, 045007 (2008).

[7] K. Wright, K. M. Beck, S. Debnath, J. Amini, Y. Nam, N. Grzesiak, J.-S. Chen, N. Pisenti, M. Chmielewski, C. Collins et al., Benchmarking an 11-qubit quantum computer, Nat. Commun. 10, 5464 (2019).

[8] D. Kielpinski, C. Monroe, and D. J. Wineland, Architecture for a large-scale ion-trap quantum computer, Nature (London) 417, 709 (2002).

[9] J. M. Pino, J. M. Dreiling, C. Figgatt, J. P. Gaebler, S. A. Moses, M. Allman, C. Baldwin, M. Foss-Feig, D. Hayes, K. Mayer et al., Demonstration of the trapped-ion quantum CCD computer architecture, Nature (London) 592, 209 (2021).

[10] I. Pogorelov, T. Feldker, C. D. Marciniak, L. Postler, G. Jacob, O. Krieglsteiner, V. Podlesnic, M. Meth, V. Negnevitsky, M. Stadler et al., Compact ion-trap quantum computing demonstrator, PRX Quantum 2, 020343 (2021).

[11] M. Rowe, A. Ben-Kish, B. Demarco, D. Leibfried, V. Meyer, J. Beall, J. Britton, J. Hughes, W. Itano, B. Jelenković et al., Transport of quantum states and separation of ions in a dual RF ion trap, Quantum Inf. Comput. 2, 257 (2002).

[12] F. Splatt, M. Harlander, M. Brownnutt, F. Zähringer, R. Blatt, and W. Hänsel, Deterministic reordering of ^{40}Ca$^+$ ions in a linear segmented Paul trap, New J. Phys. 11, 103008 (2009).

[13] J. P. Home, D. Hanneke, J. D. Jost, J. M. Amini, D. Leibfried, and D. J. Wineland, Complete methods set for scalable ion trap quantum information processing, Science 325, 1227 (2009).

[14] W. Hensinger, S. Olmschenk, D. Stick, D. Hucul, M. Yeo, M. Acton, L. Deslauriers, C. Monroe, and J. Rabchuk, T-junction ion trap array for two-dimensional ion shuttling, storage, and manipulation, Appl. Phys. Lett. 88, 034101 (2006).

[15] R. B. Blakestad, C. Ospelkaus, A. P. VanDevender, J. M. Amini, J. Britton, D. Leibfried, and D. J. Wineland, High-Fidelity Transport of Trapped-Ion Qubits through an **X**-Junction Trap Array, Phys. Rev. Lett. 102, 153002 (2009).

[16] R. B. Blakestad, C. Ospelkaus, A. P. VanDevender, J. H. Wesenberg, M. J. Biercuk, D. Leibfried, and D. J. Wineland, Near-ground-state transport of trapped-ion qubits through a multidimensional array, Phys. Rev. A 84, 032314 (2011).

[17] K. Wright, J. M. Amini, D. L. Faircloth, C. Volin, S. C. Doret, H. Hayden, C. Pai, D. W. Landgren, D. Denison, T. Killian et al., Reliable transport through a microfabricated **X**-junction surface-electrode ion trap, New J. Phys. 15, 033004 (2013).

[18] J. M. Amini, H. Uys, J. H. Wesenberg, S. Seidelin, J. Britton, J. J. Bollinger, D. Leibfried, C. Ospelkaus, A. P. Van Devender, and D. J. Wineland, Toward scalable ion traps for quantum information processing, New J. Phys. 12, 033031 (2010).

[19] D. L. Moehring, C. Highstrete, D. Stick, K. M. Fortier, R. Haltli, C. Tigges, and M. G. Blain, Design, fabrication and experimental demonstration of junction surface ion traps, New J. Phys. 13, 075018 (2011).

[20] G. Shu, G. Vittorini, A. Buikema, C. S. Nichols, C. Volin, D. Stick, and K. R. Brown, Heating rates and ion-motion control in a Y-junction surface-electrode trap, Phys. Rev. A 89, 062308 (2014).

[21] C. Decaroli, R. Matt, R. Oswald, C. J. Axline, M. Ernzer, J. Flannery, S. Ragg, and J. P. Home, Design, fabrication and characterisation of a micro-fabricated stacked-wafer segmented ion trap with two X-junctions, Quantum Sci. Technol. 6, 044001 (2021).

[22] C. Zhang, K. K. Mehta, and J. P. Home, Optimization and implementation of a surface-electrode ion trap junction, New J. Phys. 24, 073030 (2022).

[23] See Supplemental Material at http://link.aps.org/supplemental/10.1103/PhysRevLett.130.173202 for more details of the surface trap design, waveform generation

method, and a plot of the numerical simulation results, which includes Refs. [24–26].

[24] J. Chiaverini, R. Blakestad, J. Britton, J. Jost, C. Langer, D. Leibfried, R. Ozeri, and D. Wineland, Surface-electrode architecture for ion-trap quantum information processing, Quantum Inf. Comput. **5**, 419 (2005).

[25] E. Torrontegui, S. Ibáñez, X. Chen, A. Ruschhaupt, D. Guéry-Odelin, and J. G. Muga, Fast atomic transport without vibrational heating, Phys. Rev. A **83**, 013415 (2011).

[26] D. J. Berkeland, J. D. Miller, J. C. Bergquist, W. M. Itano, and D. J. Wineland, Minimization of ion micromotion in a Paul trap, J. Appl. Phys. **83**, 5025 (1998).

[27] J. Dreesand W. Paul, Beschleunigung von Elektronen in einem Plasmabetatron, Z. Phys. **180**, 340 (1964).

[28] D. Hucul, M. Yeo, S. Olmschenk, C. Monroe, W. Hensinger, and J. Rabchuk, On the transport of atomic ions in linear and multidimensional ion trap arrays, Quantum Inf. Comput. **8,** 501 (2008).

[29] J. H. Wesenberg, Ideal intersections for radio-frequency trap networks, Phys. Rev. A **79**, 013416 (2009).

[30] C. Monroe, D. M. Meekhof, B. E. King, S. R. Jefferts, W. M. Itano, D. J. Wineland, and P. Gould, Resolved-Sideband Raman Cooling of a Bound Atom to the 3D Zero-Point Energy, Phys. Rev. Lett. **75**, 4011 (1995).

[31] M. Palmero, R. Bowler, J. P. Gaebler, D. Leibfried, and J. G. Muga, Fast transport of mixed-species ion chains within a Paul trap, Phys. Rev. A **90**, 053408 (2014).